NOISE SOURCE LOCALIZATION IN AN ATTENUATING MEDIUM*

HABIB AMMARI†, ELIE BRETIN‡, JOSSELIN GARNIER§, AND ABDUL WAHAB‡

Abstract. In this paper we consider the problem of reconstructing the spatial support of noise sources from boundary measurements using cross correlation techniques. We consider media with and without attenuation and provide efficient imaging functionals in both cases. We also discuss the case where the noise sources are spatially correlated. We present numerical results to show the viability of the different proposed imaging techniques.

AMS subject classifications. 35L05, 35R30; Secondary 47A52, 65J20

Key words. Passive imaging, wave propagation, attenuation

1. Introduction. The main objective of this paper is to present an original approach for detecting the spatial support of noise sources in an attenuating electromagnetic or acoustic medium. The main application envisaged by our work concerns robotic sound or microwave noise source localization and tracking; see, for instance, [12, 13, 14, 15, 21]. It is a quite challenging problem to build an autonomous robotic system for finding, investigating, and modeling ambient electromagnetic or sound noise sources in the environment. On the other hand, a robot can be a rather significant source of electromagnetic and/or acoustic noise. Detecting or hiding the robot to reduce the risk of being detected is also another challenging problem. As will be seen in this paper, at least two robots have to be used in order to locate noise sources by cross correlation.

Passive imaging from noisy signals has been a very active field. It has been shown that the Green's function of the wave equation in an inhomogeneous medium can be estimated by cross correlating the signals emitted by ambient noise sources and recorded by a passive sensor array [7, 17, 18]. The idea has been used for travel time estimation and background velocity estimation in geophysical contexts, and also for passive sensor imaging of reflectors [9, 10], which consists of backpropagating or migrating the cross correlation matrix of the recorded signals. The relation between the cross correlation of ambient noise signals recorded at two observation points and the Green's function between these two points can be proved using the Helmholtz-Kirchhoff identity when the ambient noise sources surround the observation region [5, 20] or using stationary phase arguments in the high-frequency regime when the support ambient noise sources are spatially limited [9, 19].

In [11] the noise source imaging problem is analyzed in a high-frequency asymptotic regime and the support of the noise sources is identified with a special Radon transform. Here we shall consider a general context in non-attenuating and attenuating media. In attenuating media, one can think to first pre-process the data as originally done in [4] and then backpropagate the cross correlation of the pre-processed data in a non-attenuating medium. However, this seems impossible because the recorded data are very long and usually contain a huge amount of additional measurement noise. Instead, we backpropagate the cross correlation of the recorded data with a regularized version of the adjoint operator. Our main

*This work was supported by the ERC Advanced Grant Project MULTIMOD–267184.

†Department of Mathematics and Applications, Ecole Normale Supérieure, 45 Rue d'Ulm, 75005 Paris, France (habib.ammari@ens.fr).

‡Centre de Mathématiques Appliquées, CNRS UMR 7641, École Polytechnique, 91128 Palaiseau, France (bretin@cmap.polytechnique.fr, wahab@cmap.polytechnique.fr).

§Laboratoire de Probabilités et Modèles Aléatoires & Laboratoire Jacques-Louis Lions, Université Paris VII, 75205 Paris Cedex 13, France (garnier@math.jussieu.fr). Corresponding author.

tool is a generalization to attenuating media of the Helmholtz-Kirchhoff identity. Moreover, we address the problem of localizing spatially correlated noise sources. In particular, we consider two specific examples: an extended distribution of locally correlated sources and a collection of correlated point sources. We build functionals from the cross correlation that are capable of first locating the noise sources and then estimating the correlation structure between them.

The paper is organized as follows. In Section 2, we introduce a model problem and recall the definition of cross correlation. In Section 3, we consider noise source localization in non-attenuating media. We propose and analyze a weighted imaging functional for locating noise sources which is based on backpropagating the cross correlation of the data and estimating the power spectral density of the noise sources. In Section 4, we consider the thermo-viscous wave model to incorporate the attenuation effect in wave propagation. Our strategy for localizing the noise sources is to backpropagate the cross correlation with a regularized version of the adjoint wave operator. We contrast this with the approach consisting of first preprocessing the data before backrpopagating the cross correlation. In Section 5, we address the impact of spatial correlation on noise source localization. Some numerical illustrations to highlight the potential of proposed imaging functionals in the considered contexts are presented. Finally, the paper ends with a short discussion and a conclusion.

2. Media Without Attenuation. Let us consider the scalar wave equation in a d-dimensional open medium

$$\begin{cases} \dfrac{1}{c^2(\boldsymbol{x})}\dfrac{\partial^2 p}{\partial t^2}(t,\boldsymbol{x}) - \Delta p(t,\boldsymbol{x}) = n(t,\boldsymbol{x}), \quad (t,\boldsymbol{x}) \in \mathbb{R}\times\mathbb{R}^d, \\ p(t,\boldsymbol{x}) = \dfrac{\partial p(t,\boldsymbol{x})}{\partial t} = 0, \qquad\qquad\qquad\qquad t \ll 0, \end{cases} \tag{2.1}$$

where $d = 2$ or 3, $c(\boldsymbol{x})$ is a positive smooth function bounded from below and above, and the term $n(t,\boldsymbol{x})$ models a distribution of noise sources that is compactly supported in a smooth bounded domain Ω. The function $c(\boldsymbol{x})$ is supposed to be equal to one outside a large ball. Furthermore, we assume that $n(t,\boldsymbol{x})$ is a stationary (in time) Gaussian process with mean zero and covariance function

$$\langle n(t,\boldsymbol{x})n(s,\boldsymbol{y})\rangle = F(t-s)K(\boldsymbol{x})\delta(\boldsymbol{x}-\boldsymbol{y}), \tag{2.2}$$

where δ is the Dirac mass at the origin, the brackets stand for the statistical average, F is the time covariance of the noise signals (its Fourier transform is the power spectral density) and K characterizes the spatial support of the sources. The function K is the quantity we want to identify from the data set $\{p(t,\boldsymbol{x}), t\in[0,T], \boldsymbol{x}\in\partial\Omega\}$ recorded at the surface of the domain Ω.

We need the following notation. Let $\hat{v}(\omega)$ denote the Fourier transform of a function $v(t)$:

$$\hat{v}(\omega) = \int_{\mathbb{R}} v(t)\exp(i\omega t)dt.$$

We also introduce

$$G(t,\boldsymbol{x},\boldsymbol{y}) = \frac{1}{2\pi}\int_{\mathbb{R}} \hat{G}(\omega,\boldsymbol{x},\boldsymbol{y})\exp(-i\omega t)d\omega,$$

where $\hat{G}$ is the outgoing fundamental solution to the Helmholtz equation $-(\Delta + \omega^2/c(\boldsymbol{x}))$ in $\mathbb{R}^d$:

$$\big(\Delta_{\boldsymbol{x}} + \frac{\omega^2}{c^2(\boldsymbol{x})}\big)\hat{G}(\omega, \boldsymbol{x}, \boldsymbol{y}) = -\delta(\boldsymbol{x} - \boldsymbol{y}) \quad \text{in } \mathbb{R}^d.$$

The time-dependent Green's function is causal in the sense that $G(t, \boldsymbol{x}, \boldsymbol{y}) = 0$ for all $t \leq 0$.

We observe the waves at the surface of the domain Ω and we compute the empirical cross correlation:

$$C_T(\tau, \boldsymbol{x}, \boldsymbol{y}) = \frac{1}{T}\int_0^T p(t, \boldsymbol{x})p(t + \tau, \boldsymbol{y})dt, \qquad \boldsymbol{x}, \boldsymbol{y} \in \partial\Omega. \tag{2.3}$$

If the recording time window is long enough then the empirical cross correlation is equivalent to the statistical cross correlation [9]

$$\begin{aligned} C(\tau, \boldsymbol{x}, \boldsymbol{y}) &= \langle p(t, \boldsymbol{x})p(t + \tau, \boldsymbol{y})\rangle \\ &= \frac{1}{2\pi}\int_{\mathbb{R}}\Big[\int_\Omega \overline{\hat{G}}(\omega, \boldsymbol{x}, \boldsymbol{z})\hat{G}(\omega, \boldsymbol{y}, \boldsymbol{z})K(\boldsymbol{z})d\boldsymbol{z}\Big]\hat{F}(\omega)\exp(-i\omega\tau)\,d\omega. \end{aligned} \tag{2.4}$$

Note that the statistical cross correlation contains all the information about the data. Indeed the data set $\{p(t, \boldsymbol{x}), t \in [0, T], \boldsymbol{x} \in \partial\Omega\}$ has stationary Gaussian distribution with mean zero, so that its statistical distribution is fully characterized by the cross correlation.

3. Source Localization. We aim at identifying the source function K. The idea is to backpropagate the cross correlation of the data, which contains all the accessible information about the source distribution. The imaging functional for source localization is given by

$$\mathcal{I}(\boldsymbol{z}^S) = \int_{\mathbb{R}}\iint_{\partial\Omega\times\partial\Omega}\hat{G}(\omega, \boldsymbol{x}, \boldsymbol{z}^S)\overline{\hat{G}}(\omega, \boldsymbol{y}, \boldsymbol{z}^S)\hat{C}_T(\omega, \boldsymbol{x}, \boldsymbol{y})d\sigma(\boldsymbol{x})d\sigma(\boldsymbol{y})d\omega \tag{3.1}$$

for the search point $\boldsymbol{z}^S \in \Omega$. Here $\hat{C}$ is the Fourier transform of C defined by (2.4). Definition (3.1) is equivalent to

$$\mathcal{I}(\boldsymbol{z}^S) = 2\pi\iint_{\partial\Omega\times\partial\Omega}\Big[\int_0^\infty\int_0^\infty G(t, \boldsymbol{x}, \boldsymbol{z}^S)G(s, \boldsymbol{y}, \boldsymbol{z}^S)C_T(s - t, \boldsymbol{x}, \boldsymbol{y})dtds\Big]d\sigma(\boldsymbol{x})d\sigma(\boldsymbol{y}). \tag{3.2}$$

By (2.4) and Helmholtz-Kirchhoff identity [2]

$$\int_{\partial\Omega}\hat{G}(\omega, \boldsymbol{x}, \boldsymbol{y})\overline{\hat{G}}(\omega, \boldsymbol{z}, \boldsymbol{y})d\sigma(\boldsymbol{y}) \simeq \frac{1}{\omega}\mathrm{Im}\big\{\hat{G}(\omega, \boldsymbol{x}, \boldsymbol{z})\big\}, \tag{3.3}$$

which holds as $|\boldsymbol{x} - \boldsymbol{y}|$ and $|\boldsymbol{z} - \boldsymbol{y}|$ are large enough compared to the wavelength $2\pi/\omega$, we find that

$$\mathcal{I}(\boldsymbol{z}^S) \simeq \int_{\mathbb{R}}\int_\Omega \frac{\hat{F}(\omega)}{\omega^2}\mathrm{Im}\big\{\hat{G}(\omega, \boldsymbol{z}^S, \boldsymbol{z})\big\}^2 K(\boldsymbol{z})d\boldsymbol{z}d\omega.$$

This gives the following proposition.

PROPOSITION 3.1. *The imaging functional (3.1) gives the source function K up to a smoothing operator, i.e.,*

$$\mathcal{I}(\boldsymbol{z}^S) \simeq \int_\Omega \mathcal{Q}(\boldsymbol{z}^S, \boldsymbol{z})K(\boldsymbol{z})d\boldsymbol{z} \tag{3.4}$$

with the smoothing kernel $\mathcal{Q}$ defined by

$$\mathcal{Q}(\boldsymbol{z}^S, \boldsymbol{z}) = \int_{\mathbb{R}} \frac{\hat{F}(\omega)}{\omega^2} \mathrm{Im}\big\{\hat{G}(\omega, \boldsymbol{z}^S, \boldsymbol{z})\big\}^2 d\omega. \tag{3.5}$$

In view of Proposition 3.1, the resolution of the imaging functional $\mathcal{I}$ is determined by the kernel $\mathcal{Q}(\boldsymbol{z}^S, \boldsymbol{z})$. High-frequency components are penalized in this functional because of the factor ω^{-2} and therefore, the resolution is limited. In order to achieve a better resolution, we shall modify the imaging functional to make its smoothing kernel as close as possible from a Dirac distribution $\delta(\boldsymbol{z}^S - \boldsymbol{z})$. We should be aware that enhancing the high-frequency components may cause instability in the imaging procedure. In the next subsection we introduce a weighted imaging algorithm where the weight is chosen in terms of estimations of the power spectral density of the noise sources.

3.1. Two- and Three-Dimensional Homogeneous Media. In this subsection we first show that the smoothing operator is a simple convolution operator in the case of a three-dimensional homogeneous background with $c(\boldsymbol{x}) \equiv 1$ in $\mathbb{R}^3$. Indeed, the Green's function is

$$G(t, \boldsymbol{x}, y) = \frac{1}{4\pi|\boldsymbol{x} - \boldsymbol{y}|} \delta\big(t - |\boldsymbol{x} - \boldsymbol{y}|\big)$$

and hence the imaging functional takes the simple form

$$\mathcal{I}(\boldsymbol{z}^S) = \frac{1}{8\pi} \iint_{\partial\Omega\times\partial\Omega} \frac{1}{|\boldsymbol{x} - \boldsymbol{z}^S|\,|\boldsymbol{y} - \boldsymbol{z}^S|} C_T\big(|\boldsymbol{y} - \boldsymbol{z}^S| - |\boldsymbol{x} - \boldsymbol{z}^S|, \boldsymbol{x}, \boldsymbol{y}\big) d\sigma(\boldsymbol{x}) d\sigma(\boldsymbol{y}).$$

We also have

$$\frac{1}{\omega}\mathrm{Im}\big\{\hat{G}(\omega, \boldsymbol{z}^S, \boldsymbol{z})\big\} = \frac{1}{4\pi}\mathrm{sinc}\big(\omega|\boldsymbol{z} - \boldsymbol{z}^S|\big)$$

and therefore, the smoothing operator is a convolution and the imaging functional (3.1) has the form

$$\mathcal{I}(\boldsymbol{z}^S) \simeq \int_\Omega Q(\boldsymbol{z}^S - \boldsymbol{z}) K(\boldsymbol{z}) d\boldsymbol{z}$$

with the convolution kernel

$$Q(\boldsymbol{z}) = \frac{1}{16\pi^2} \int_{\mathbb{R}} \hat{F}(\omega) \mathrm{sinc}^2\big(\omega|\boldsymbol{z}|\big) d\omega.$$

In a two-dimensional homogeneous medium, the convolution kernel has the form

$$Q(\boldsymbol{z}) = \frac{1}{16} \int_{\mathbb{R}} \frac{\hat{F}(\omega)}{\omega^2} J_0^2\big(\omega|\boldsymbol{z}|\big) d\omega,$$

where J_0 is the Bessel function of the first kind and of order zero.

The presence of the factor ω^{-2} indicates that a frequency-dependent weight should be used (as explained below) in order to avoid this singularity that amplifies the low-frequency components, or that the backpropagation should be carried out with the time-derivative of the Green's function, so that the factor ω^{-2} is cancelled.

The power spectral density of the noise sources plays a smoothing role in the kernel Q while we would like this kernel to be as close as possible to a Dirac distribution. The idea for an improved functional is based on the estimation of the power spectral density of the noise sources. Let us introduce

$$\mathcal{F}(\omega) = \int_{\partial\Omega} \hat{C}_T(\omega, \boldsymbol{x}, \boldsymbol{x}) d\sigma(\boldsymbol{x}). \tag{3.6}$$

The power spectral density $\mathcal{F}(\omega)$ can be estimated from the data. However one must pay attention to the fact that the time-harmonic quantity $\hat{C}_T$ is not statistically stable, but it has a small frequency correlation radius of the order of $1/T$, where T is the recording time defined in (2.3) [9]. The time-dependent quantity C_T is stable because it is an integral over many uncorrelated frequency components. In fact is a well-known and general problem that the variance of the periodogram remains positive whatever the duration of the recorded signals. Therefore one must average the empirical estimation (3.6) over moving frequency windows large enough to ensure statistical stability and small enough to capture the variations of the power spectral density $\hat{F}(\omega)$. This means that the width $\Delta\omega$ of the moving frequency window should be larger than $1/T$, but smaller than the noise bandwidth:

$$\tilde{\mathcal{F}}(\omega) = \frac{1}{\Delta\omega} \int_{\omega-\Delta\omega/2}^{\omega+\Delta\omega/2} \int_{\partial\Omega} \hat{C}_T(\omega', \boldsymbol{x}, \boldsymbol{x}) d\sigma(\boldsymbol{x}) d\omega'.$$

Using once again Helmholtz-Kirchhoff identity, one can see that $\hat{F}(\omega)$ can be estimated by $\tilde{\mathcal{F}}(\omega)$:

$$\tilde{\mathcal{F}}(\omega) \simeq \hat{F}(\omega) \int_{\Omega} \frac{\mathrm{Im}\big\{\hat{G}(\omega, \boldsymbol{z}, \boldsymbol{z})\big\}}{\omega} K(\boldsymbol{z}) d\boldsymbol{z}.$$

In a three-dimensional homogeneous medium with $c(\boldsymbol{x}) \equiv 1$, we have

$$\frac{\mathrm{Im}\big\{\hat{G}(\omega, \boldsymbol{z}, \boldsymbol{z})\big\}}{\omega} = \frac{1}{4\pi}$$

and $\tilde{\mathcal{F}}(\omega)$ is proportional to the power spectral density of the noise sources:

$$\tilde{\mathcal{F}}(\omega) \simeq K_0 \hat{F}(\omega), \qquad K_0 = \frac{1}{4\pi} \int_{\Omega} K(\boldsymbol{z}) d\boldsymbol{z}.$$

Let us introduce a weight function $W(\omega)$ and the weighted imaging functional $\mathcal{I}_W$ as

$$\mathcal{I}_W(\boldsymbol{z}^S) = \int_{\mathbb{R}} \frac{W(\omega)}{\tilde{\mathcal{F}}(\omega)} \iint_{\partial\Omega\times\partial\Omega} \hat{G}(\omega, \boldsymbol{x}, \boldsymbol{z}^S) \overline{\hat{G}}(\omega, \boldsymbol{y}, \boldsymbol{z}^S) \hat{C}_T(\omega, \boldsymbol{x}, \boldsymbol{y}) d\sigma(\boldsymbol{x}) d\sigma(\boldsymbol{y}) d\omega. \tag{3.7}$$

PROPOSITION 3.2. *In a three-dimensional homogeneous background with $c(\boldsymbol{x}) \equiv 1$, the weigted imaging functional (3.7) satisfies*

$$\mathcal{I}_W(\boldsymbol{z}^S) = \int_{\Omega} Q_W(\boldsymbol{z}^S - \boldsymbol{z}) \frac{K(\boldsymbol{z})}{K_0} d\boldsymbol{z} \tag{3.8}$$

with

$$Q_W(\boldsymbol{z}) = \frac{1}{16\pi^2} \int_{\mathbb{R}} W(\omega) \mathrm{sinc}^2\big(\omega|\boldsymbol{z}|\big) d\omega. \tag{3.9}$$

In fact, the weight function $W(\omega)$ should be supported in the estimated band width $(-\omega_{\max}, \omega_{\max})$ of the recorded noise signals otherwise the ratio $W(\omega)/\tilde{\mathcal{F}}(\omega)$ in (3.7) makes no sense. The idea is to choose $W(\omega)$ so that the convolution kernel (called also the point spread function) Q_W is as close as possible to a Dirac distribution.

In a two-dimensional homogeneous medium, it is easy to check that (3.8) holds with

$$K_0 = \frac{1}{4}\int_\Omega K(\boldsymbol{z})d\boldsymbol{z},$$

and

$$Q_W(\boldsymbol{z}) = \frac{1}{16}\int_{\mathbb{R}} \frac{W(\omega)}{\omega^2} J_0^2\big(\omega|\boldsymbol{z}|\big)d\omega. \tag{3.10}$$

The Fourier transform of the kernel Q_W is then

$$\hat{Q}_W(\boldsymbol{k}) = \frac{1}{2|\boldsymbol{k}|^3}\int_{1/2}^{\infty} \frac{W(|\boldsymbol{k}|u)}{u^2(4u^2-1)^{1/2}}du. \tag{3.11}$$

To prove (3.11) we use [1, formula 6.522.11]

$$\int_0^\infty xJ_0^2(ax)J_0(bx)dx = \frac{2}{\pi b(4a^2-b^2)^{1/2}}\mathbf{1}_{0<b<2a},$$

where $\mathbf{1}$ denotes the characteristic function, to get

$$\int_{\mathbb{R}^2} J_0^2(\omega|\boldsymbol{z}|)\exp(i\boldsymbol{z}\cdot\boldsymbol{k})\,d\boldsymbol{z} = \frac{4}{|\boldsymbol{k}|(4\omega^2-|\boldsymbol{k}|^2)^{1/2}}\mathbf{1}_{|\boldsymbol{k}|<2|\omega|}.$$

Substituting into

$$\hat{Q}_W(\boldsymbol{k}) = \frac{1}{16}\int_{\mathbb{R}}\int_{\mathbb{R}^2} \frac{W(\omega)}{\omega^2} J_0^2(\omega|\boldsymbol{z}|)\exp(i\boldsymbol{z}\cdot\boldsymbol{k})\,d\boldsymbol{z}d\omega, \tag{3.12}$$

gives the desired formula (3.11).

With formulas (3.9) and (3.10) in hand, recalling the closure relations [16]

$$\int_0^{+\infty} \omega J_0(\omega|\boldsymbol{z}|)^2\,d\omega = \frac{1}{|\boldsymbol{z}|}\delta(\boldsymbol{z}), \tag{3.13}$$

and

$$\int_0^{+\infty} \omega^2 \mathrm{sinc}(\omega|\boldsymbol{z}|)^2\,d\omega = \frac{1}{|\boldsymbol{z}|^2}\delta(\boldsymbol{z}), \tag{3.14}$$

which hold in the sense of distributions, shows that a potential candidate for the filter $W(\omega)$ should be

$$W(\omega) = \begin{cases} |\omega|^3\mathbf{1}_{|\omega|<\omega_{\max}} & \text{for } d=2, \\ \omega^2\mathbf{1}_{|\omega|<\omega_{\max}} & \text{for } d=3, \end{cases}$$

where $(-\omega_{\max}, \omega_{\max})$ is the estimated support of $\tilde{\mathcal{F}}(\omega)$. In particular, for $d=2$, we have

$$\hat{Q}_W(\boldsymbol{k}) = \frac{\omega_{\max}}{4|\boldsymbol{k}|}\Big(1-\frac{|\boldsymbol{k}|^2}{4\omega_{\max}^2}\Big)^{1/2}\mathbf{1}_{|\boldsymbol{k}|\le 2\omega_{\max}}, \qquad Q_W(\boldsymbol{z}) = \frac{\omega_{\max}^2}{4}\Big[J_0^2\big(\omega_{\max}|\boldsymbol{z}|\big)+J_1^2\big(\omega_{\max}|\boldsymbol{z}|\big)\Big].$$

3.2. Backpropagation in a Two-Dimensional Medium. We show in this subsection how it is possible to implement a parallel version of the imaging functional. Here we do not assume that $c(\boldsymbol{x}) \equiv 1$. For the sake of simplicity we consider only the two-dimensional case. Similar calculations can be carried out in three dimensions using spherical harmonics. We set Ω to be the disk with center at zero and radius one and denote by $C(\tau, \theta, \theta')$ the cross correlations measured between the points $\boldsymbol{e}_\theta$ and $\boldsymbol{e}_{\theta'}$, with $\boldsymbol{e}_\theta = (\cos\theta, \sin\theta)$. We can expand the cross correlation in the basis $\exp(in\theta)$:

$$C_T(\tau, \theta, \theta') = \sum_{n,m\in\mathbb{Z}} c_{n,m}(\tau) \exp(in\theta + im\theta'),$$

where

$$c_{n,m}(\tau) = \frac{1}{4\pi^2} \int_0^{2\pi} \int_0^{2\pi} C_T(\tau, \theta, \theta') \exp(-in\theta - im\theta')\, d\theta d\theta'.$$

Then the imaging functional takes the form

$$\mathcal{I}(\boldsymbol{z}^S) = 2\pi \sum_{n,m\in\mathbb{Z}} \int_0^\infty \int_0^\infty p_n(t, \boldsymbol{z}^S) p_m(s, \boldsymbol{z}^S) c_{n,m}(s-t) ds dt,$$

or

$$\mathcal{I}(\boldsymbol{z}^S) = \sum_{n,m\in\mathbb{Z}} \int_{\mathbb{R}} \hat{p}_n(\omega, \boldsymbol{z}^S) \overline{\hat{p}_m}(\omega, \boldsymbol{z}^S) \hat{c}_{n,m}(\omega) d\omega,$$

where

$$p_n(t, \boldsymbol{z}) = \int_0^{2\pi} G(t, \boldsymbol{e}_\theta, \boldsymbol{z}) \exp(in\theta)\, d\theta$$

is the solution to the problem

$$\begin{cases} \dfrac{1}{c^2(\boldsymbol{x})} \dfrac{\partial^2 p_n}{\partial t^2}(t, \boldsymbol{x}) - \Delta p_n(t, \boldsymbol{x}) = f_n(\boldsymbol{x}) \delta_{\partial\Omega}(\boldsymbol{x}) \delta_0(t), & (t, \boldsymbol{x}) \in [0, \infty) \times \mathbb{R}^2, \\ p_n(t, \boldsymbol{x}) = \dfrac{\partial p_n(t, \boldsymbol{x})}{\partial t} = 0, & t = 0. \end{cases}$$

Here $\delta_{\partial\Omega}$ is the Dirac mass at $\partial\Omega$ and $f_n(\boldsymbol{x}) = (x_1 + ix_2)^n$ for $\boldsymbol{x} = (x_1, x_2)$ so that $\exp(in\theta) = f_n(\cos\theta, \sin\theta)$. Note that $f_{-n} = \overline{f_n}$ so that $p_{-n} = \overline{p_n}$. In practice the functional is truncated as follows

$$\mathcal{I}_N(\boldsymbol{z}^S) = 2\pi \sum_{n,m=-N}^{N} \int_0^\infty \int_0^\infty p_n(t, \boldsymbol{z}^S) p_m(s, \boldsymbol{z}^S) c_{n,m}(s-t) ds dt.$$

This version of the imaging functional can be implemented in a parallel way: on the one hand, one needs to compute the functions $p_n(t, \boldsymbol{z})$ for $n = 0, \ldots, N$, $t > 0$, $\boldsymbol{z} \in \Omega$ (we do not need to know the data), which requires to solve N wave equations; on the other hand one computes the coefficients $c_{n,m}(\tau)$, $n, m = 0, \ldots, N$, $\tau \in \mathbb{R}$ from the data set. However, the memory cost is huge, because one needs to store the full time-space solutions of the N

wave equations (at least the solutions in the search region).

A numerical alternative consists of using a PDE description of time-reversal algorithm [2, 3, 8]. Indeed, note that

$$\begin{aligned}\mathcal{I}(\boldsymbol{z}^S) &= \int_{\mathbb{R}}\int_{\partial\Omega}\int_{\partial\Omega} \hat{G}(\omega,\boldsymbol{x},\boldsymbol{z}^S)\overline{\hat{G}}(\omega,\boldsymbol{x},\boldsymbol{z}^S)\hat{C}_T(\omega,\boldsymbol{x},\boldsymbol{y})d\sigma(\boldsymbol{x})d\sigma(\boldsymbol{y})d\omega \\ &= \int_{\mathbb{R}}\int_{\partial\Omega}\int_{\partial\Omega} \hat{G}(\omega,\boldsymbol{x},\boldsymbol{z}^S)\overline{\hat{G}}(\omega,\boldsymbol{x},\boldsymbol{z}^S)\overline{\hat{p}}(\omega,\boldsymbol{x})\hat{p}(\omega,\boldsymbol{y})d\sigma(\boldsymbol{x})d\sigma(\boldsymbol{y})d\omega \\ &= \int_{\mathbb{R}}\left|\int_{\partial\Omega}\hat{G}(\omega,\boldsymbol{x},\boldsymbol{z}^S)\overline{\hat{p}}(\omega,\boldsymbol{x})d\sigma(\boldsymbol{x})\right|^2 d\omega = 2\pi\int_0^T v(t,\boldsymbol{z}^s)^2 dt,\end{aligned}$$

where the function v is expressed in the form

$$v(\boldsymbol{x},t) = \int_0^T v_s(t,\boldsymbol{x})ds,$$

and v_s is the solution of

$$\begin{cases}\frac{1}{c^2(\boldsymbol{x})}\frac{\partial^2 v_s(t,\boldsymbol{x})}{\partial t^2} - \Delta v_s(t,\boldsymbol{x}) = p(T-s,\boldsymbol{x})\delta_{\partial\Omega}(\boldsymbol{x})\delta(t-s) \\ v_s(t,\boldsymbol{x}) = 0, \quad \partial_t v_s(t,\boldsymbol{x}) = 0 \quad \text{for all } t < s.\end{cases}$$

More generally, the imaging functional $\mathcal{I}_W(\boldsymbol{z}^S)$ can be obtained by applying $\mathcal{I}(\boldsymbol{z}^S)$ on the filtered data $\tilde{p}(t,\boldsymbol{x})$, obtained as

$$\hat{\tilde{p}}(\omega,\boldsymbol{x}) = \sqrt{\frac{W(\omega)}{\tilde{\mathcal{F}}(\omega)}}\hat{p}(\omega,\boldsymbol{x}).$$

In this paper, we used this method to perform some numerical experiments.

3.3. Numerical Simulations. In this subsection we first describe the discretization of the noise sources and recorded signals that can be used in numerical simulations. We introduce a regular grid of points $(\boldsymbol{x}_k)_{k=1,\dots,N_x}$ with grid step h_x covering the support of K and a regular grid of positive frequencies $(\omega_j)_{j=1,\dots,N_\omega}$ with grid step h_ω covering the support of $\hat{F}$. The noise source term can be discretized in space as

$$n(t,\boldsymbol{x}) = \frac{1}{\pi^{d/2}h_x^{d/2}}\sum_{k=1}^{N_x}\exp(-\frac{|\boldsymbol{x}_k-\boldsymbol{x}|^2}{h_x^2})\,K(\boldsymbol{x}_k)^{1/2}n_k(t), \tag{3.15}$$

where the processes $n_k(t)$ are independent stationary Gaussian processes with mean zero and covariance function $F(t)$. They can be discretized in time/frequency as

$$n_k(t) = \frac{(2h_\omega)^{1/2}}{\pi^{1/2}}\mathrm{Re}\Big\{\sum_{j=1}^{N_\omega} Z_{j,k}\hat{F}(\omega_j)^{1/2}\exp(-i\omega_j t)\Big\},$$

where $Z_{k,j} = A_{k,j} + iB_{k,j}$, $A_{k,j}$ and $B_{k,j}$ being independent Gaussian random variables with mean zero and variance $1/2$ (so that $\langle Z_{k,j}^2\rangle = 0$ and $\langle |Z_{k,j}|^2\rangle = 1$). We have indeed

(remember that $\hat{F}$ is even and nonnegative real-valued)

$$\begin{aligned}\langle n_k(t)n_k(t+\tau)\rangle &= \frac{h_\omega}{2\pi}\Big[\sum_{j=1}^{N_\omega}\hat{F}(\omega_j)\exp(-i\omega_j\tau)+\sum_{j=1}^{N_\omega}\hat{F}(-\omega_j)\exp(i\omega_j\tau)\Big]\\ &\simeq \frac{1}{2\pi}\int_{\mathbb{R}}\hat{F}(\omega)\exp(-i\omega\tau)\,d\omega = F(\tau),\end{aligned}$$

provided h_ω is small enough, and

$$\begin{aligned}\langle n(t,\boldsymbol{x})n(t+\tau,\boldsymbol{y})\rangle &= \frac{1}{\pi^d h_x^d}\exp(-\frac{|\boldsymbol{x}-\boldsymbol{y}|^2}{2h_x^2})\sum_{k=1}^{N_x}\exp(-2\frac{|\frac{\boldsymbol{x}+\boldsymbol{y}}{2}-\boldsymbol{x}_k|^2}{h_x^2})\,K(\boldsymbol{x}_k)F(\tau)\\ &\simeq \frac{1}{\pi^d h_x^{2d}}\exp(-\frac{|\boldsymbol{x}-\boldsymbol{y}|^2}{2h_x^2})\int_{\mathbb{R}^d}\exp(-2\frac{|\frac{\boldsymbol{x}+\boldsymbol{y}}{2}-\boldsymbol{z}|^2}{h_x^2})K(\boldsymbol{z})d\boldsymbol{z}F(\tau)\\ &= \frac{1}{\pi^d h_x^{2d}}\exp(-\frac{|\boldsymbol{x}-\boldsymbol{y}|^2}{2h_x^2})\int_{\mathbb{R}^d}\exp(-2\frac{|\boldsymbol{z}|^2}{h_x^2})K\big(\frac{\boldsymbol{x}+\boldsymbol{y}}{2}-\boldsymbol{z}\big)d\boldsymbol{z}F(\tau)\\ &\simeq \frac{1}{(2\pi)^{d/2}h_x^d}\exp(-\frac{|\boldsymbol{x}-\boldsymbol{y}|^2}{2h_x^2})K\big(\frac{\boldsymbol{x}+\boldsymbol{y}}{2}\big)F(\tau)\\ &\simeq \delta(\boldsymbol{x}-\boldsymbol{y})K(\boldsymbol{x})F(\tau),\end{aligned}$$

provided h_x is small enough.

It is also possible to take

$$n(t,\boldsymbol{x}) = h_x^{d/2}\sum_{k=1}^{N_x}\delta(\boldsymbol{x}_k-\boldsymbol{x})K(\boldsymbol{x}_k)^{1/2}n_k(t)$$

instead of (3.15), which is the simplest model for numerical simulations (a collection of uncorrelated point sources). In these conditions the recorded noise signal at $\boldsymbol{x}$ is

$$p(t,\boldsymbol{x}) = \frac{(2h_\omega)^{1/2}h_x^{d/2}}{\pi^{1/2}}\mathrm{Re}\Big\{\sum_{j=1}^{N_\omega}\sum_{k=1}^{N_x}\hat{G}(\omega_j,\boldsymbol{x},\boldsymbol{x}_k)\hat{F}(\omega_j)^{1/2}K(\boldsymbol{x}_k)^{1/2}Z_{j,k}\exp(-i\omega_j t)\Big\}$$

and the statistical cross correlation is (remember $\hat{G}(-\omega,\boldsymbol{x},\boldsymbol{y}) = \overline{\hat{G}}(\omega,\boldsymbol{x},\boldsymbol{y})$)

$$\begin{aligned}C(\tau,\boldsymbol{x},\boldsymbol{y}) = \frac{h_\omega h_x^d}{2\pi}\Big[&\sum_{j=1}^{N_\omega}\sum_{k=1}^{N_x}\overline{\hat{G}}(\omega_j,\boldsymbol{x},\boldsymbol{x}_k)\hat{G}(\omega_j,\boldsymbol{y},\boldsymbol{x}_k)\hat{F}(\omega_j)K(\boldsymbol{x}_k)\exp(-i\omega_j\tau)\\ &+\sum_{j=1}^{N_\omega}\sum_{k=1}^{N_x}\overline{\hat{G}}(-\omega_j,\boldsymbol{x},\boldsymbol{x}_k)\hat{G}(-\omega_j,\boldsymbol{y},\boldsymbol{x}_k)\hat{F}(-\omega_j)K(\boldsymbol{x}_k)\exp(i\omega_j\tau)\Big]\\ \simeq \frac{1}{2\pi}\int_{\mathbb{R}}\int_{\Omega}&\overline{\hat{G}}(\omega,\boldsymbol{x},\boldsymbol{z})\hat{G}(\omega,\boldsymbol{y},\boldsymbol{z})\hat{F}(\omega)K(\boldsymbol{z})\exp(-i\omega\tau)\,d\boldsymbol{z}d\omega.\end{aligned}$$

For all numerical experiments presented in this paper, the set Ω is assumed to be a disk centered at the origin and of radius one. The function F is chosen in the form

$$\hat{F}(\omega) = \exp\left(-\pi\frac{\omega^2}{\omega_{\max}^2}\right). \tag{3.16}$$

The solution v_s of the equation

$$\frac{1}{c^2(\boldsymbol{x})}\frac{\partial^2 v_s(t,\boldsymbol{x})}{\partial t^2} - \Delta v_s(t,\boldsymbol{x}) = p(T-s,\boldsymbol{x})\delta_{\partial\Omega}(\boldsymbol{x})\delta(t-s)$$

is computed on a larger box $\Omega \subset Q = [-L/2, L/2]^2$. We use a Fourier spectral approach coupled with a Perfectly Matched Layer technique to simulate a free outgoing interface on ∂Q. The boundary $\partial\Omega$ is discretized using steps of discretization given by $h_t = T/N_t$ and $h_x = L/N_x$.

Figure 3.1 shows some numerical reconstructions of the source location K using the imaging functionals $\mathcal{I}$ and $\mathcal{I}_W$ for $W(\omega) = |\omega|^3 \mathbf{1}_{|\omega|<\omega_{\max}}$. The first line corresponds to the case of well separated point sources. It turns out that both imaging functionals give an efficient reconstruction of the source K. The second line corresponds to the case of extended sources (five localized Gaussian peaks). We observe in this case that the second imaging functional $\mathcal{I}_W$ gives a better reconstruction of K. We expect that this observation is a consequence of the factor ω^{-2} which appears in the kernel associated to $\mathcal{I}$ and penalizes the high-frequency components of the image.

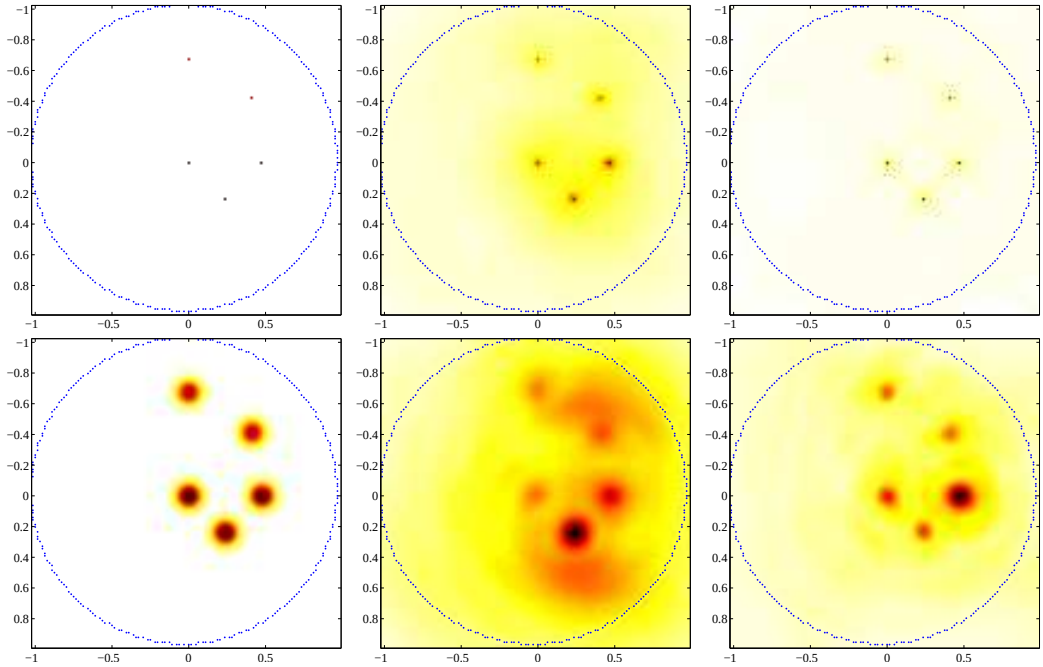

FIG. 3.1. *Test 1: non-attenuating medium with $T = 8$, $\omega_{\max} = 1000$, $N_x = 2^8$, and $N_t = 2^{11}$. Top line: five point sources; bottom line: five extended sources. Left: $K(\boldsymbol{x})$; middle: reconstruction of K using $\mathcal{I}$; right: reconstruction of K using $\mathcal{I}_W$ with $W(\omega) = |\omega|^3 \mathbf{1}_{|\omega|<\omega_{\max}}$.*

Figure 3.2 presents estimations of the power spectral density. Averaging (3.6) over moving frequency windows yields a statistically stable estimation.

4. Localization of Sources in Attenuating Media. In this section, we consider the thermo-viscous wave model to incorporate the attenuation effect in wave propagation.

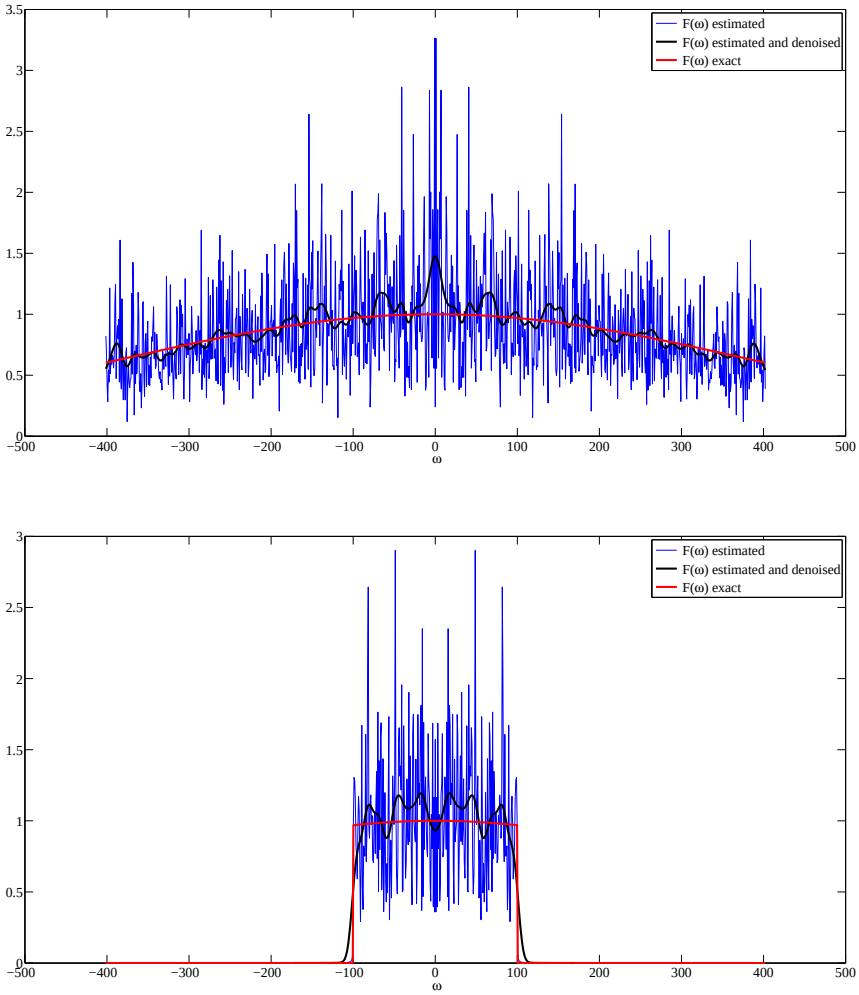

FIG. 3.2. *Estimations of the power spectral density with and without averaging over a moving frequency window. Top figure:* $\hat{F}(\omega) = \exp\left(-\pi\omega^2/\omega_{\max}^2\right)$ *(as in (3.16)) with* $\omega_{\max} = 1000$. *Bottom figure:* $\hat{F}(\omega) = \mathbf{1}_{|\omega|\leq 100} \exp\left(-\pi\omega^2/\omega_{\max}^2\right)$.

Let p_a be the solution of the problem

$$\begin{cases} \dfrac{1}{c^2(\boldsymbol{x})}\dfrac{\partial^2 p_a}{\partial t^2}(t,\boldsymbol{x}) - \Delta p_a(t,\boldsymbol{x}) - a\dfrac{\partial}{\partial t}\Delta p_a(t,\boldsymbol{x}) = n(t,\boldsymbol{x}), & (t,\boldsymbol{x}) \in \mathbb{R}\times\mathbb{R}^d, \\ p_a(t,\boldsymbol{x}) = \dfrac{\partial p_a}{\partial t}(t,\boldsymbol{x}) = 0, & t \ll 0. \end{cases}$$

Again, the problem is to reconstruct the source function K from the data set $\{p_a(t,\boldsymbol{x}), t \in [0,T], \boldsymbol{x} \in \partial\Omega\}$ recorded at the surface of the domain Ω, or more exactly from the empirical cross correlation $C_{T,a}$ defined as in (2.3).

We introduce the fundamental solution $\hat{G}_a(\omega, \boldsymbol{x}, y)$ of the Helmholtz equation

$$\frac{\omega^2}{c^2(\boldsymbol{x})}\hat{G}_a(\omega, \boldsymbol{x}, \boldsymbol{y}) + (1 - ia\omega)\Delta_{\boldsymbol{x}}\hat{G}_a(\omega, \boldsymbol{x}, \boldsymbol{y}) = -\delta(\boldsymbol{y} - \boldsymbol{x}).$$

It is given by

$$\hat{G}_a(\omega, \boldsymbol{x}, \boldsymbol{y}) = \frac{\kappa_a(\omega)^2}{\omega^2}\hat{G}(\kappa_a(\omega), \boldsymbol{x}, \boldsymbol{y}) \tag{4.1}$$

in terms of the non-attenuating Green's function $\hat{G}(\omega, \boldsymbol{x}, \boldsymbol{y}) = \hat{G}_0(\omega, \boldsymbol{x}, \boldsymbol{y})$, with

$$\kappa_a(\omega) = \frac{\omega}{\sqrt{1 - ia\omega}}.$$

When the recording time T is long enough, the empirical cross correlation $C_{T,a}$ is equivalent to the statistical cross correlation

$$\begin{aligned} C_a(\tau, \boldsymbol{x}, \boldsymbol{y}) &= \langle p_a(t, \boldsymbol{x}) p_a(t + \tau, \boldsymbol{y})\rangle \\ &= \frac{1}{2\pi}\int_{\mathbb{R}}\Big[\int_{\Omega}\overline{\hat{G}_a}(\omega, \boldsymbol{x}, \boldsymbol{z})\hat{G}_a(\omega, \boldsymbol{y}, \boldsymbol{z})K(\boldsymbol{z})d\boldsymbol{z}\Big]\hat{F}(\omega)\exp(-i\omega\tau)\,d\omega. \end{aligned}$$

Our strategy to localize the sources is to backpropagate the cross correlation with a regularized version of the adjoint propagator.

4.1. Hemholtz-Kirchhoff Identity. Our main tool for studying noise source localization in attenuating media is the following result. It is a generalization to attenuating media of the Helmholtz-Kirchhoff identity (3.3).

LEMMA 4.1. *If Ω is a ball with large radius (compared to the wavelength $2\pi/\omega$) and $c(\boldsymbol{x})$ is equal to one outside the ball then*

$$\int_{\partial\Omega}\hat{G}_{-a}(\omega, \boldsymbol{x}, \boldsymbol{z}^S)\overline{\hat{G}_a}(\omega, \boldsymbol{x}, \boldsymbol{z})d\sigma(\boldsymbol{x}) \simeq \frac{1}{2i\overline{\kappa_a(\omega)}(1 + ia\omega)}\big(\hat{G}_{-a}(\omega, \boldsymbol{z}, \boldsymbol{z}^S) - \overline{\hat{G}_a}(\omega, \boldsymbol{z}, \boldsymbol{z}^S)\big). \tag{4.2}$$

We also have

$$\begin{aligned} &(1 + a^2\omega^2)\kappa_{a,r}(\omega)\int_{\partial\Omega}\hat{G}_a(\omega, \boldsymbol{x}, \boldsymbol{z}^S)\overline{\hat{G}_a}(\omega, \boldsymbol{x}, \boldsymbol{z})d\sigma(\boldsymbol{x}) \\ &+a\omega^3\int_{\Omega}c^{-2}(\boldsymbol{z})\hat{G}_a(\omega, \boldsymbol{x}, \boldsymbol{z}^S)\overline{\hat{G}_a}(\omega, \boldsymbol{x}, \boldsymbol{z})d\boldsymbol{x} \\ &\qquad\simeq \mathrm{Im}\big(\hat{G}_a(\omega, \boldsymbol{z}^S, \boldsymbol{z})\big) - a\omega\mathrm{Re}\big(\hat{G}_a(\omega, \boldsymbol{z}^S, \boldsymbol{z})\big) \end{aligned} \tag{4.3}$$

with

$$\kappa_{a,r}(\omega) = \mathrm{Re}(\kappa_a(\omega)) = \frac{\omega}{\sqrt{2}\sqrt{1 + a^2\omega^2}}\sqrt{\sqrt{1 + a^2\omega^2} + 1}. \tag{4.4}$$

Proof. It is a consequence of Green's theorem and the fact that $\overline{\kappa_a(\omega)} = \kappa_{-a}(\omega)$. More precisely, we consider the equations

$$-\frac{\omega^2}{c^2(\boldsymbol{x})}\hat{G}_{-a}(\omega, \boldsymbol{x}, \boldsymbol{z}^S) - (1 + ia\omega)\Delta_{\boldsymbol{x}}\hat{G}_{-a}(\omega, \boldsymbol{x}, \boldsymbol{z}^S) = \delta(\boldsymbol{z}^S - \boldsymbol{x}) \tag{4.5}$$

and

$$-\frac{\omega^2}{c^2(\boldsymbol{x})}\overline{\hat{G}_a(\omega,\boldsymbol{x},\boldsymbol{z})}-(1+ia\omega)\Delta_{\boldsymbol{x}}\overline{\hat{G}_a(\omega,\boldsymbol{x},\boldsymbol{z})}=\delta(\boldsymbol{z}-\boldsymbol{x}). \tag{4.6}$$

We then multiply (4.5) by $\overline{\hat{G}_a(\omega,\boldsymbol{x},\boldsymbol{z})}$ and (4.6) by $\hat{G}_{-a}(\omega,\boldsymbol{x},\boldsymbol{z}^S)$, subtract these two equations from each other, integrate over Ω and apply Green's divergence theorem. □

Note the presence of the volume integral in (4.3) which shows that the adjoint Green's function $\hat{G}_{-a}$ should be used for backpropagation and not the Green's function $\hat{G}_a$. The imaging functional for source localization should be

$$\mathcal{I}(\boldsymbol{z}^S)=\int_{\mathbb{R}}\iint_{\partial\Omega\times\partial\Omega}\hat{G}_{-a}(\omega,\boldsymbol{x},\boldsymbol{z}^S)\overline{\hat{G}_{-a}}(\omega,\boldsymbol{y},\boldsymbol{z}^S)\hat{C}_{T,a}(\omega,\boldsymbol{x},\boldsymbol{y})d\sigma(\boldsymbol{x})d\sigma(\boldsymbol{y})d\omega \tag{4.7}$$

for the search point $\boldsymbol{z}^S\in\Omega$. However, the backpropagation uses the adjoint operator $\hat{G}_{-a}(\omega,\boldsymbol{x},\boldsymbol{z}^S)$ that has an exponentially growing part, since it can be seen from

$$\kappa_{a,i}(\omega)=\mathrm{Im}(\kappa_a(\omega))=\frac{|\omega|\mathrm{sgn}(a)}{\sqrt{2}\sqrt{1+a^2\omega^2}}\sqrt{\sqrt{1+a^2\omega^2}-1}, \tag{4.8}$$

where sgn denotes the sign function, that $\kappa_{-a,i}(\omega)$ is negative. Thus we should use a regularized version of the form

$$\mathcal{I}_\rho(\boldsymbol{z}^S)=\int_{|\omega|\le\rho}\iint_{\partial\Omega\times\partial\Omega}\hat{G}_{-a}(\omega,\boldsymbol{x},\boldsymbol{z}^S)\overline{\hat{G}_{-a}}(\omega,\boldsymbol{y},\boldsymbol{z}^S)\hat{C}_{T,a}(\omega,\boldsymbol{x},\boldsymbol{y})d\sigma(\boldsymbol{x})d\sigma(\boldsymbol{y})d\omega, \tag{4.9}$$

where ρ is a cut-off frequency. Using Lemma 4.1 we obtain the following result.

PROPOSITION 4.2. *The regularized imaging functional (4.9) satisfies*

$$\mathcal{I}_\rho(\boldsymbol{z}^S)=\int_\Omega\mathcal{Q}_\rho(\boldsymbol{z}^S,\boldsymbol{z})K(\boldsymbol{z})d\boldsymbol{z} \tag{4.10}$$

with

$$\mathcal{Q}_\rho(\boldsymbol{z}^S,\boldsymbol{z})=\int_{|\omega|\le\rho}\frac{\hat{F}(\omega)}{4\omega^2(1+a^2\omega^2)^{1/2}}\left|\hat{G}_{-a}(\omega,\boldsymbol{z},\boldsymbol{z}^S)-\overline{\hat{G}_a}(\omega,\boldsymbol{z},\boldsymbol{z}^S)\right|^2d\omega. \tag{4.11}$$

The next subsection will show how to calibrate the cut-off parameter ρ in order to get a stable imaging functional.

4.2. Three-Dimensional Homogeneous Medium. Using the explicit expression of the homogeneous Green's function we get the following lemma.

LEMMA 4.3. *The Green's function $\hat{G}_{-a}(\omega,\boldsymbol{x},\boldsymbol{y})$ is given by*

$$\hat{G}_{-a}(\omega,\boldsymbol{x},\boldsymbol{y})=\frac{\kappa_{-a}(\omega)^2}{\omega^2}\hat{G}(\kappa_{-a}(\omega),\boldsymbol{x},\boldsymbol{y})\quad\text{with }\hat{G}(\omega,\boldsymbol{x},\boldsymbol{y})=\frac{\exp(i\omega|\boldsymbol{x}-\boldsymbol{y}|)}{4\pi|\boldsymbol{x}-\boldsymbol{y}|}.$$

If Ω is a ball with large radius (compared to the wavelength), then we have

$$\begin{aligned}&\int_{\partial\Omega}\hat{G}_{-a}(\omega,\boldsymbol{x},\boldsymbol{z}^S)\overline{\hat{G}_a}(\omega,\boldsymbol{x},\boldsymbol{z})d\sigma(\boldsymbol{x})\\&\simeq\frac{\kappa_{a,r}(\omega)}{4\pi\omega(1+ia\omega)^{3/2}}\mathrm{sinc}\big(\kappa_{a,r}(\omega)|\boldsymbol{z}^S-\boldsymbol{z}|\big)\cosh\big(\kappa_{a,i}(\omega)|\boldsymbol{z}^S-\boldsymbol{z}|\big)\\&\quad-i\frac{\kappa_{a,i}(\omega)}{4\pi\omega(1+ia\omega)^{3/2}}\cos\big(\kappa_{a,r}(\omega)|\boldsymbol{z}^S-\boldsymbol{z}|\big)\mathrm{sinhc}\big(\kappa_{a,i}(\omega)|\boldsymbol{z}^S-\boldsymbol{z}|\big),\end{aligned} \tag{4.12}$$

where $\mathrm{sinc}(r) = \sin(r)/r$ *and* $\mathrm{sinhc}(r) = \sinh(r)/r$.

The adjoint operator $\hat{G}_{-a}(\omega, \boldsymbol{x}, \boldsymbol{z}^S)$ grows exponentially as $\exp(\kappa_{a,i}(\omega)|\boldsymbol{z}^S - \boldsymbol{x}|)$. This term should not be much larger than one, otherwise noise terms would be amplified in the backpropagation. Since $\kappa_{a,i}(\omega)$ grows like $a\omega^2/2$ for $a|\omega| < 1$, (and as $(|\omega|/(2a))^{1/2}$ for $a|\omega| > 1$), one should not backpropragate the high-frequency components, with frequencies larger than $(a\,\mathrm{diam}(\Omega))^{-1/2}$, where diam denotes the diameter. This limitation also allows to neglect the exponential term in the right-hand side of (4.12) and to claim that identity (4.12) gives a localized kernel that has the form of a sinc with a width of the order of the wavelength.

The imaging functional for source localization is given by (4.9). The cut-off frequency ρ should be of the order of $(a\,\mathrm{diam}(\Omega))^{-1/2}$. By (4.12) we arrive at the following proposition.

PROPOSITION 4.4. *In a three-dimensional homogeneous background with* $c(\boldsymbol{x}) \equiv 1$ *and* $a > 0$*, the regularized imaging functional (4.9) satisfies*

$$\mathcal{I}_\rho(\boldsymbol{z}^S) \simeq \int_\Omega Q_\rho(\boldsymbol{z}^S - \boldsymbol{z}) K(\boldsymbol{z}) d\boldsymbol{z} \tag{4.13}$$

with

$$\begin{aligned} Q_\rho(\boldsymbol{z}) = {} & \frac{1}{16\pi^2} \int_{|\omega|\le\rho} \hat{F}(\omega) \frac{\sqrt{1+a^2\omega^2}+1}{2(1+a^2\omega^2)^{5/2}} \mathrm{sinc}^2\big(\kappa_{a,r}(\omega)|\boldsymbol{z}|\big) d\omega \\ & + \frac{1}{16\pi^2} \int_{|\omega|\le\rho} \hat{F}(\omega) \frac{\sqrt{1+a^2\omega^2}-1}{2(1+a^2\omega^2)^{5/2}} \mathrm{sinhc}^2\big(\kappa_{a,i}(\omega)|\boldsymbol{z}|\big) d\omega. \end{aligned} \tag{4.14}$$

The first term in (4.14) gives the peak centered at zero in the convolution kernel Q_ρ, with a width of the order of ρ^{-1}. The second term is responsible for the instability of the imaging functional (since it is exponentially growing). In order to make it small compared to the peak, we should cut the high frequencies and choose ρ smaller than $(a\mathrm{diam}(\Omega))^{-1/2}$. This means that, at the expense of a loss in resolution, the imaging functional can be stable.

4.3. Backpropagation in a Two-Dimensional Medium. Here we do not assume that $c(\boldsymbol{x}) \equiv 1$. We consider that Ω is the disk centered at the origin and of radius one. We expand the cross correlation as in Subsection 3.2:

$$C_{T,a}(\tau, \theta, \theta') = \sum_{n,m\in\mathbb{Z}} c_{n,m}(\tau) \exp(in\theta + im\theta'),$$

where

$$c_{n,m}(\tau) = \frac{1}{4\pi^2} \int_0^{2\pi} \int_0^{2\pi} C_{T,a}(\tau, \theta, \theta') \exp(-in\theta - im\theta')\, d\theta d\theta'.$$

Then the imaging functional takes the form

$$\mathcal{I}(\boldsymbol{z}^S) = 2\pi \sum_{n,m\in\mathbb{Z}} \int_0^\infty \int_0^\infty p_{-a,n}(t, \boldsymbol{z}^S) p_{-a,m}(s, \boldsymbol{z}^S) c_{n,m}(s-t) ds dt,$$

or

$$\mathcal{I}(\boldsymbol{z}^S) = \sum_{n,m\in\mathbb{Z}} \int_{\mathbb{R}} \hat{p}_{-a,n}(\omega, \boldsymbol{z}^S) \overline{\hat{p}_{-a,m}}(\omega, \boldsymbol{z}^S) \hat{c}_{n,m}(\omega) d\omega,$$

where

$$p_{-a,n}(t,\boldsymbol{z}) = \int_0^{2\pi} G_{-a}(t,\boldsymbol{e}_\theta,\boldsymbol{z})\exp(in\theta)\,d\theta$$

is the solution to the problem

$$\begin{cases} \Big[\dfrac{1}{c^2(\boldsymbol{x})}\dfrac{\partial^2}{\partial t^2} - \Delta + a\dfrac{\partial}{\partial t}\Delta\Big]p_{-a,n}(t,\boldsymbol{x}) = f_n(\boldsymbol{x})\delta_{\partial\Omega}(\boldsymbol{x})\delta(t), \quad (t,\boldsymbol{x}) \in [0,\infty)\times\mathbb{R}^2, \\ p_{-a,n}(t,\boldsymbol{x}) = \dfrac{\partial p_{-a,n}(t,\boldsymbol{x})}{\partial t} = 0, \qquad\qquad t = 0. \end{cases}$$

As pointed out in [4], this adjoint problem is ill-posed. We need to regularize the high frequencies. The regularized imaging functional (4.9) can be expressed as

$$\mathcal{I}_\rho(\boldsymbol{z}^S) = 2\pi \sum_{n,m\in\mathbb{Z}} \int_0^\infty \int_0^\infty p_{-a,n,\rho}(t,\boldsymbol{z}^S)p_{-a,m,\rho}(s,\boldsymbol{z}^S)c_{n,m}(s-t)dsdt$$

or

$$\begin{aligned} \mathcal{I}_\rho(\boldsymbol{z}^S) &= \sum_{n,m\in\mathbb{Z}} \int_{\mathbb{R}} \hat{p}_{-a,n,\rho}(\omega,\boldsymbol{z}^S)\overline{\hat{p}_{-a,m,\rho}}(\omega,\boldsymbol{z}^S)\hat{c}_{n,m}(\omega)d\omega \\ &= \sum_{n,m\in\mathbb{Z}} \int_{|\omega|\le\rho} \hat{p}_{-a,n}(\omega,\boldsymbol{z}^S)\overline{\hat{p}_{-a,m}}(\omega,\boldsymbol{z}^S)\hat{c}_{n,m}(\omega)d\omega, \end{aligned}$$

where

$$\hat{p}_{-a,n,\rho}(\omega,\boldsymbol{z}) = \hat{p}_{-a,n}(\omega,\boldsymbol{z})\mathbf{1}_{|\omega|\le\rho}.$$

REMARK 4.5. *The function $p_{-a,n,\rho}(t,\boldsymbol{z})$ can be identified as the solution to the problem*

$$\begin{cases} \Big[\dfrac{1}{c^2(\boldsymbol{x})}\dfrac{\partial^2}{\partial t^2} - \Delta + a\dfrac{\partial}{\partial t}\Delta\Big]p_{-a,n,\rho}(t,\boldsymbol{x}) = f_n(\boldsymbol{x})\delta_{\partial\Omega}(\boldsymbol{x})S_\rho\big[\delta\big](t), \quad (t,\boldsymbol{x}) \in [0,\infty)\times\mathbb{R}^2, \\ p_{-a,n,\rho}(t,\boldsymbol{x}) = \dfrac{\partial p_{-a,n,\rho}(t,\boldsymbol{x})}{\partial t} = 0, \qquad\qquad t = 0, \end{cases}$$

where S_ρ is the operator defined by

$$S_\rho\big[\phi\big](t) = \frac{1}{2\pi}\int_{|\omega|\le\rho} \hat{\phi}(\omega)\exp(-i\omega t)\,d\omega.$$

Note also that the functional $\mathcal{I}_\rho$ can be expressed in the form

$$\mathcal{I}_\rho(\boldsymbol{z}) = \int_0^T v_{-a,\rho}(t,\boldsymbol{z})dt,$$

where

$$v_{-a,\rho}(t,\boldsymbol{z}) = \int_0^T v_{s,-a,\rho}(t,\boldsymbol{z})ds,$$

and $v_{s,-a,\rho}$ being defined as the solution of the equation

$$\left[\frac{1}{c^2(\boldsymbol{x})}\frac{\partial^2}{\partial t^2} - \Delta + a\frac{\partial}{\partial t}\Delta\right] v_{s,-a,\rho}(t,\boldsymbol{x}) = p(T-s,\boldsymbol{x})\delta_{\partial\Omega}(\boldsymbol{x})S_\rho\left[\delta\right](t-s).$$

4.4. Remark on the Backpropagation in a Non-Attenuating Medium of Pre-Processed Data. An idea that seems interesting is to try to build a regularized imaging functional as in the case of a source term that is a Dirac distribution in time [4]. This can be done by first regularizing the data and then backpropagating it in the non-attenuating medium.

On the one hand, it is not possible to do this to the data themselves, since the recorded signals are very long and usually contain a huge amount of additional measurement noise (which disappears when one computes the cross correlation). Indeed, we have

$$\hat{C}_a(\omega, \boldsymbol{x}, \boldsymbol{y}) = \hat{F}(\omega) \int_\Omega \overline{\hat{G}_a(\omega, \boldsymbol{x}, \boldsymbol{z})} \hat{G}_a(\omega, \boldsymbol{y}, \boldsymbol{z}) K(\boldsymbol{z}) d\boldsymbol{z}, \tag{4.15}$$

and, although (4.1) holds, formula (4.15) is not in the form

$$\hat{C}_a(\omega, \boldsymbol{x}, \boldsymbol{y}) = \hat{F}(\omega) \frac{|\kappa_a(\omega)|^4}{\omega^4} \int_\Omega \hat{H}(\kappa_a(\omega), \boldsymbol{x}, \boldsymbol{y}, \boldsymbol{z}) K(\boldsymbol{z}) d\boldsymbol{z}.$$

In fact, we have

$$\begin{aligned}\hat{C}_a(\omega, \boldsymbol{x}, \boldsymbol{y}) = \hat{F}(\omega) \frac{|\kappa_a(\omega)|^4}{\omega^4} \int_0^\infty \int_0^\infty \int_\Omega K(\boldsymbol{z}) G(s, \boldsymbol{x}, \boldsymbol{z}) G(s+v, \boldsymbol{y}, \boldsymbol{z}) d\boldsymbol{z} \exp(-2\kappa_{a,i}(\omega) s) ds \\ \times \exp(i\kappa_a(\omega) v) dv.\end{aligned}$$

The damping $\exp(-2\kappa_{a,i}(\omega)s)$ is quite problematic. It implies that the compensation of the attenuation can only be carried out -approximately- for a given target point $\boldsymbol{z}^S$, which means using the adjoint Green's function or equivalently, backpropagating in an amplifying medium.

4.5. Numerical Experiments. Figure 4.1 presents some numerical source reconstructions in attenuating media. Each line respectively corresponds to the attenuation coefficient $a = 0.0005$, $a = 0.001$, and $a = 0.002$. In the first column, the sources are localized by applying the imaging functional $\mathcal{I}_W$. As expected, the attenuation affects the image quality. In the second and the third columns of Figure 4.1, we use the functional $\mathcal{I}_\rho$ with $\rho = 7.5$ and $\rho = 15$, respectively. The reconstructions are improved, but as illustrated in the last figure of the third line, this technique is quite instable in the case of a too large attenuation coefficient a.

5. Localization of Correlated Sources. In the previous sections we have considered the case in which the noise sources are spatially uncorrelated, which translates in the fact that the covariance function (2.2) is delta-correlated in space. In this section we would like to address the impact of spatial correlation in the source localization. First we will address the general problem and then we will consider two specific examples: an extended distribution of locally correlated sources and a collection of correlated point sources.

5.1. Spatially Correlated Sources. We assume in this section that the noise source term $n(t, \boldsymbol{x})$ is a stationary (in time) Gaussian process with mean zero and covariance function

$$\langle n(t, \boldsymbol{x}) n(s, \boldsymbol{y}) \rangle = F(t-s) \Gamma(\boldsymbol{x}, \boldsymbol{y}), \tag{5.1}$$

where F is the time covariance of the noise signals and Γ characterizes the spatial support and covariance of the sources. The function Γ is the quantity we want to identify from

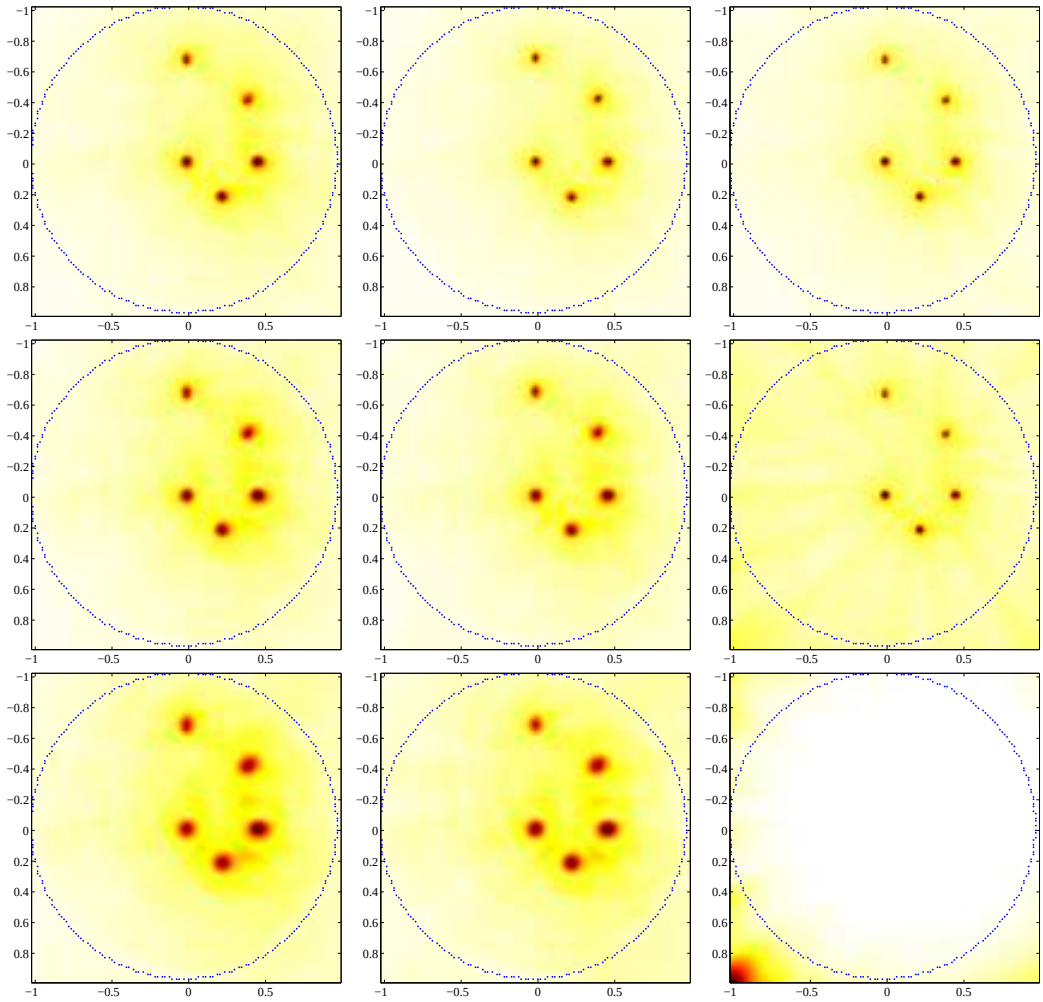

FIG. 4.1. *Test 2: five point sources in attenuating medium with* $T = 8$, $\omega_{\max} = 1000$, $N_x = 2^8$, *and* $N_t = 2^{11}$. *From top to bottom:* $a = 0.0005$, $a = 0.001$, *and* $a = 0.002$. *From left to right:* $\mathcal{I}_W$, $\mathcal{I}_\rho$ *with* $\rho = 7.5$, *and* $\mathcal{I}_\rho$ *with* $\rho = 15$.

the data set $\{p(t, \boldsymbol{x}), t \in [0, T], \boldsymbol{x} \in \partial\Omega\}$ recorded at the surface of the domain Ω. We are primary interested in the support of Γ, but we would like also to extract information about the covariance structure of the noise sources.

The empirical cross correlation (2.3) is self-averaging as in the delta-correlated case and becomes equivalent to the statistical cross correlation C when the recording time $T \to \infty$, where

$$C(\tau, \boldsymbol{x}, \boldsymbol{y}) = \frac{1}{2\pi} \int_{\mathbb{R}} \Big[\iint_{\Omega\times\Omega} \overline{\hat{G}}(\omega, \boldsymbol{x}, \boldsymbol{z}) \hat{G}(\omega, \boldsymbol{y}, \boldsymbol{z}') \Gamma(\boldsymbol{z}, \boldsymbol{z}') d\boldsymbol{z} d\boldsymbol{z}' \Big] \hat{F}(\omega) \exp(-i\omega\tau)\, d\omega. \quad (5.2)$$

We can build two functionals from the cross correlation. The first one is $\mathcal{I}$ defined by (3.1) and aims at estimating the support of the noise sources. The second one aims at

estimating the covariance function Γ and is defined by

$$\mathcal{J}(\boldsymbol{z}^S, \boldsymbol{z}^{S'}) = \int_{\mathbb{R}} \iint_{\partial\Omega\times\partial\Omega} \hat{G}(\omega, \boldsymbol{x}, \boldsymbol{z}^S)\overline{\hat{G}}(\omega, \boldsymbol{y}, \boldsymbol{z}^{S'})\hat{C}_T(\omega, \boldsymbol{x}, \boldsymbol{y})d\sigma(\boldsymbol{x})d\sigma(\boldsymbol{y})d\omega. \tag{5.3}$$

Note that we have $\mathcal{I}(\boldsymbol{z}^S) = \mathcal{J}(\boldsymbol{z}^S, \boldsymbol{z}^S)$. Using Helmholtz-Kirchhoff formula, we obtain the following result.

PROPOSITION 5.1. *The functional (5.3) satisfies*

$$\mathcal{J}(\boldsymbol{z}^S, \boldsymbol{z}^{S'}) = \iint_{\Omega\times\Omega} \Psi(\boldsymbol{z}^S, \boldsymbol{z}^{S'}, \boldsymbol{z}, \boldsymbol{z}')\Gamma(\boldsymbol{z}, \boldsymbol{z}')d\boldsymbol{z}d\boldsymbol{z}'$$

with

$$\Psi(\boldsymbol{z}^S, \boldsymbol{z}^{S'}, \boldsymbol{z}, \boldsymbol{z}') = \int_{\mathbb{R}} \frac{\hat{F}(\omega)}{\omega^2}\mathrm{Im}\hat{G}(\omega, \boldsymbol{z}, \boldsymbol{z}^S)\mathrm{Im}\hat{G}(\omega, \boldsymbol{z}', \boldsymbol{z}^{S'})d\omega.$$

In particular, in a three-dimensional homogeneous medium we have

$$\Psi(\boldsymbol{z}^S, \boldsymbol{z}^{S'}, \boldsymbol{z}, \boldsymbol{z}') = \psi(\boldsymbol{z}^S - \boldsymbol{z}, \boldsymbol{z}^{S'} - \boldsymbol{z}'), \tag{5.4}$$

with

$$\psi(\boldsymbol{z}, \boldsymbol{z}') = \frac{1}{16\pi^2}\int_{\mathbb{R}} \hat{F}(\omega)\mathrm{sinc}(\omega|\boldsymbol{z}|)\mathrm{sinc}(\omega|\boldsymbol{z}'|)d\omega, \tag{5.5}$$

which shows that the convolution kernel smoothes in both $\boldsymbol{z}$ and $\boldsymbol{z}'$ the estimation of Γ by the functional $\mathcal{J}$.

5.2. An Extended Distribution of Locally Correlated Sources. Let us assume that the covariance of the noise source term is of the form

$$\Gamma(\boldsymbol{z}, \boldsymbol{z}') = K(\frac{\boldsymbol{z}+\boldsymbol{z}'}{2})\gamma(\boldsymbol{z}-\boldsymbol{z}').$$

Here, the function K characterizes the spatial support of the noise sources and γ characterizes the local covariance structure. This models an extended noise source distribution which has local correlation. Then, we find the following result.

PROPOSITION 5.2. *The functional (3.1) satisfies*

$$\mathcal{I}(\boldsymbol{z}^S) = \int_{\Omega} \Phi(\boldsymbol{z}, \boldsymbol{z}^S)K(\boldsymbol{z})d\boldsymbol{z}$$

with

$$\Phi(\boldsymbol{z}, \boldsymbol{z}^S) = \int_{\mathbb{R}} \frac{\hat{F}(\omega)}{\omega^2}\int \mathrm{Im}\hat{G}(\omega, \boldsymbol{z}+\boldsymbol{\zeta}/2, \boldsymbol{z}^S)\mathrm{Im}\hat{G}(\omega, \boldsymbol{z}-\boldsymbol{\zeta}/2, z^S)\gamma(\boldsymbol{\zeta})d\boldsymbol{\zeta}d\omega.$$

In particular, in a three-dimensional homogeneous medium we have

$$\Phi(\boldsymbol{z}, \boldsymbol{z}^S) = \phi(\boldsymbol{z} - \boldsymbol{z}^S), \tag{5.6}$$

with

$$\phi(\boldsymbol{z}) = \frac{1}{16\pi^2}\int_{\mathbb{R}} \hat{F}(\omega)\int \mathrm{sinc}(\omega|\boldsymbol{z}+\boldsymbol{\zeta}/2|)\mathrm{sinc}(\omega|\boldsymbol{z}-\boldsymbol{\zeta}/2|)\gamma(\boldsymbol{\zeta})d\boldsymbol{\zeta}d\omega. \tag{5.7}$$

This shows that we recover the function K up to a smoothing that is large when γ is far from a Dirac distribution or a narrow peak. Spatial correlation in the noise sources blur the source localization.

If the width of the function γ is smaller than $\omega_{\max}^{-1}$ where $\omega_{\max}$ is the maximal frequency of the power spectral density $\hat{F}$, then the spatial correlation of the sources play no role and we recover the results obtained in the case of delta-correlated noise sources in which the convolution kernel (5.7) is given by

$$\phi(\boldsymbol{z}) = \frac{\hat{\gamma}(\mathbf{0})}{16\pi^2} \int_{\mathbb{R}} \hat{F}(\omega) \mathrm{sinc}^2(\omega|\boldsymbol{z}|) d\omega. \tag{5.8}$$

If the width of the function γ is large and the function γ is isotropic so that $\hat{\gamma}(\boldsymbol{k}) = \tilde{\gamma}(|\boldsymbol{k}|)$, then the convolution kernel (5.7) is given by

$$\phi(\boldsymbol{z}) = 2\Big[\int_0^\infty k\tilde{\gamma}(k)dk\Big] \int_{\mathbb{R}} \frac{\hat{F}(\omega)}{\omega^2} \mathrm{sinc}(2\omega|\boldsymbol{z}|) d\omega. \tag{5.9}$$

The kernel is not nonnegative (which means that sidelobes are likely to appear). Moreover, low-frequency components are amplified, so that it is necessary to use a frequency-dependent weight or to backpropagate with the time-derivative of the Green's function in order to cancel the factor ω^{-2} in (5.9). Note that formula (5.9) follows from the substitution of the representation formula

$$\mathrm{sinc}(\omega|\boldsymbol{z}|) = \frac{1}{4\pi} \int_{\partial B(\mathbf{0},1)} \exp(i\omega \boldsymbol{z} \cdot \boldsymbol{k})\, d\sigma(\boldsymbol{k})$$

in (5.7).

5.3. A Collection of Correlated Point Sources. Let us assume that the covariance of the noise source term is of the form

$$\Gamma(\boldsymbol{z}, \boldsymbol{z}') = \sum_{i,j=1}^{N_s} \gamma_{ij} \delta(\boldsymbol{z} - \boldsymbol{z}_i) \delta(\boldsymbol{z} - \boldsymbol{z}_j),$$

where $(\gamma_{ij})_{i,j=1,\dots,N_s}$ is a symmetric nonnegative matrix. This models a collection of N_s point sources located at $\boldsymbol{z}_i$, $i = 1, \dots, N_s$, which have respective power γ_{ii}. The coefficients $\rho_{ij} = \gamma_{ij}/\sqrt{\gamma_{ii}\gamma_{jj}} \in [-1, 1]$ represent the correlations between the sources at $\boldsymbol{z}_i$ and $\boldsymbol{z}_j$. Then we find that

$$\begin{aligned} \mathcal{I}(\boldsymbol{z}^S) &= \sum_{i,j=1}^{N_s} \gamma_{ij} \int_{\mathbb{R}} \frac{\hat{F}(\omega)}{\omega^2} \mathrm{Im}\hat{G}(\omega, \boldsymbol{z}_i, \boldsymbol{z}^S) \mathrm{Im}\hat{G}(\omega, \boldsymbol{z}_j, \boldsymbol{z}^S) d\omega \\ &\simeq \sum_{i=1}^{N_s} \gamma_{ii} \mathcal{Q}(\boldsymbol{z}^S, \boldsymbol{z}_i), \end{aligned}$$

provided the sources are well separated, where $\mathcal{Q}$ is defined as in (3.5):

$$\mathcal{Q}(\boldsymbol{z}^S, \boldsymbol{z}) = \int_{\mathbb{R}} \frac{\hat{F}(\omega)}{\omega^2} \mathrm{Im}\hat{G}(\omega, \boldsymbol{z}, \boldsymbol{z}^S)^2 d\omega.$$

In particular, in a three-dimensional homogeneous medium:

$$\mathcal{Q}(\boldsymbol{z}^S, \boldsymbol{z}) = \frac{1}{16\pi^2} \int_{\mathbb{R}} \hat{F}(\omega) \mathrm{sinc}^2(\omega|\boldsymbol{z} - \boldsymbol{z}^S|) d\omega.$$

This shows that the functional $\mathcal{Q}$ indeed exhibits peaks at the locations of the noise sources.

Once the local maxima $\hat{\boldsymbol{z}}_i$, $i = 1, \ldots, N_s$, have been estimated, it is possible to estimate the correlation matrix between the noise sources by looking at the functional $\mathcal{J}$ at these points. Indeed we have

$$\mathcal{J}(\boldsymbol{z}^S, \boldsymbol{z}^{S'}) = \sum_{i,j=1}^{N_s} \gamma_{ij} \int \frac{\hat{F}(\omega)}{\omega^2} \mathrm{Im}\hat{G}(\omega, \boldsymbol{z}_i, \boldsymbol{z}^{S'}) \mathrm{Im}\hat{G}(\omega, \boldsymbol{z}_j, \boldsymbol{z}^S) d\omega.$$

Therefore,

$$\mathcal{J}(\boldsymbol{z}_i, \boldsymbol{z}_j) = \gamma_{ij} \int_{\mathbb{R}} \frac{\hat{F}(\omega)}{\omega^2} \mathrm{Im}\hat{G}(\omega, \boldsymbol{z}_i, \boldsymbol{z}_i) \mathrm{Im}\hat{G}(\omega, \boldsymbol{z}_j, \boldsymbol{z}_j) d\omega.$$

In particular, in a three-dimensional homogeneous medium, it follows that

$$\mathcal{J}(\boldsymbol{z}_i, \boldsymbol{z}_j) = \mathcal{J}_0 \gamma_{ij}, \qquad \mathcal{J}_0 = \frac{1}{16\pi^2} \int_{\mathbb{R}} \hat{F}(\omega) d\omega = \frac{1}{8\pi} F(0).$$

The estimation of correlation matrix can be important in robot sound or microwave source surveillance and tracking; see, for instance, [15].

5.4. Numerical Experiments for Identifying Correlated Noise Sources. A numerical method to compute efficiently $\mathcal{J}(\boldsymbol{z}, \boldsymbol{z}')$ follows from

$$\begin{aligned}
\mathcal{J}(\boldsymbol{z}, \boldsymbol{z}') &= \int_{\mathbb{R}} \iint_{\partial\Omega} \hat{G}(\omega, \boldsymbol{x}, \boldsymbol{z}) \overline{\hat{G}}(\omega, \boldsymbol{x}, \boldsymbol{z}') \hat{C}_T(\omega, \boldsymbol{x}, \boldsymbol{y}) d\sigma(\boldsymbol{x}) d\sigma(\boldsymbol{y}) d\omega \\
&= \int_{\mathbb{R}} \iint_{\partial\Omega} \hat{G}(\omega, \boldsymbol{x}, \boldsymbol{z}) \overline{\hat{G}}(\omega, \boldsymbol{x}, \boldsymbol{z}') \overline{\hat{p}}(\omega, \boldsymbol{x}) \hat{p}(\omega, \boldsymbol{y}) d\sigma(\boldsymbol{x}) d\sigma(\boldsymbol{y}) d\omega \\
&= \int_{\mathbb{R}} \left(\int_{\partial\Omega} \hat{G}(\omega, \boldsymbol{x}, \boldsymbol{z}) \overline{\hat{p}}(\omega, \boldsymbol{x}) d\sigma(\boldsymbol{x}) \right) \overline{\left(\int_{\partial\Omega} \hat{G}(\omega, \boldsymbol{y}, \boldsymbol{z}') \overline{\hat{p}}(\omega, \boldsymbol{y}) d\sigma(\boldsymbol{y}) \right)} d\omega \\
&= 2\pi \int_0^T v(t, \boldsymbol{z}) v(t, \boldsymbol{z}') dt,
\end{aligned}$$

where the function v can be expressed in the form

$$v(t, \boldsymbol{x}) = \int_0^T v_s(t, \boldsymbol{x}) ds,$$

and the function v_s being defined as the solution of

$$\begin{cases} \frac{1}{c^2(\boldsymbol{x})} \frac{\partial^2 v_s(t, \boldsymbol{x})}{\partial t^2} - \Delta v_s(t, \boldsymbol{x}) = p(T - s, \boldsymbol{x}) \delta_{\partial\Omega}(\boldsymbol{x}) \delta(t - s) \\ v_s(t, \boldsymbol{x}) = 0, \quad \partial_t v_s(t, \boldsymbol{x}) = 0, \quad \text{for all } t < s. \end{cases}$$

More generally, the imaging functional $\mathcal{J}_W(\boldsymbol{z}, \boldsymbol{z}')$ can be defined by applying $\mathcal{J}(\boldsymbol{z}, \boldsymbol{z}')$ on the filtered data $\tilde{p}(t, \boldsymbol{x})$ given by

$$\hat{\tilde{p}}(\omega, \boldsymbol{x}) = \sqrt{\frac{W(\omega)}{\tilde{\mathcal{F}}(\omega)}}\hat{p}(\omega, \boldsymbol{x}).$$

In Figure 5.1, we consider four point noise sources with the same power spectral density (3.16) and with the correlation matrix

$$\rho = \begin{pmatrix} 1 & \sqrt{2}/2 & \sqrt{2}/2 & 0 \\ \sqrt{2}/2 & 1 & 0 & 0 \\ \sqrt{2}/2 & 0 & 1 & 0 \\ 0 & 0 & 0 & 1 \end{pmatrix}.$$

The top-left figure presents the true distribution $K(\boldsymbol{x})$. The top-middle figure shows the reconstruction of K using the imaging functional $\mathcal{I}_W$. In particular, it appears that the source localization is not as efficient as in the case of uncorrelated data, but is sufficient for locating the noise sources. In the last four figures, we plot the imaging functional $\boldsymbol{z} \to \mathcal{J}_W(\boldsymbol{z}_i, \boldsymbol{z})$ for each source $\boldsymbol{z}_i$, which allows us to get the following estimate of the cross correlation matrix:

$$\hat{\rho} = \begin{pmatrix} 1.000 & 0.733 & 0.701 & 0.061 \\ 0.733 & 1.000 & 0.049 & 0.061 \\ 0.701 & 0.049 & 1.000 & 0.030 \\ 0.061 & 0.061 & 0.030 & 1.000 \end{pmatrix}$$

Note that each correlation is found quite well ($\sqrt{2}/2 \simeq 0.707$). To conclude, some numerical results associated with the localization of extended Gaussian sources are also shown in Figure 5.2, which shows the same agreement between theoretical and numerical results as in the case of oint sources.

6. Conclusion. In this work, efficient weighted imaging algorithms for locating noise sources by cross correlation techniques have been introduced. We have provided a regularization approach to correct the effect of attenuation. We have successfully addressed the impact of spatial correlation in the noise source localization problem by designing appropriate imaging functionals. Here, we have assumed that the attenuation coefficient is homogeneous and known a priori. However, in practical situations, this is not the case and an estimation of attenuation coefficient is necessary. This would be the subject of a further investigation.

REFERENCES

[1] M. Abramowitz and I. Stegun, *Handbook of Mathematical Functions*, Dover Publications, New York, 1965.

[2] H. Ammari, *An Introduction to Mathematics of Emerging Biomedical Imaging*, Mathematics & Applications, Vol. 62, Springer-Verlag, Berlin, 2008.

[3] H. Ammari, E. Bretin, V. Jugnon, and A. Wahab, Photoacoustic imaging for attenuating acoustic media, in *Mathematical Modeling in Biomedical Imaging II*, Lecture Notes in Mathematics, Springer-Verlag, Berlin, to appear.

[4] H. Ammari, E. Bretin, J. Garnier, and A. Wahab, Time reversal in attenuating acoustic media, to appear in Contemporary Mathematics.

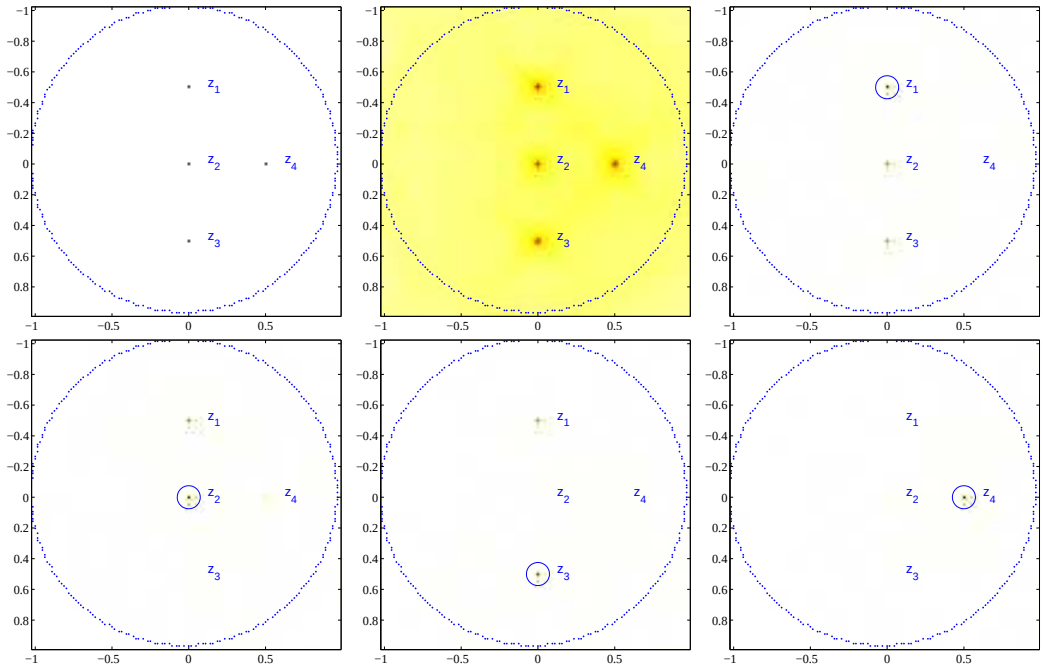

FIG. 5.1. *Test 3: four correlated source points* $(\boldsymbol{z}_j)_{j=1,\dots,4}$ *with* $T = 8$, $\omega_{\max} = 1000$, $N_x = 2^8$, *and* $N_t = 2^{11}$. *Top line:* $K(\boldsymbol{z})$ *(left),* $\mathcal{I}_W$ *with* $W(\omega) = |\omega|^3 \mathbf{1}_{|\omega|<\omega_{\max}}$ *(middle), and* $z \to \mathcal{J}_W(\boldsymbol{z}_1, \boldsymbol{z})$ *(right). Bottom line:* $\boldsymbol{z} \to \mathcal{J}_W(\boldsymbol{z}_2, \boldsymbol{z})$ *(left),* $\boldsymbol{z} \to \mathcal{J}_W(\boldsymbol{z}_3, \boldsymbol{z})$ *(middle), and* $\boldsymbol{z} \to \mathcal{J}_W(\boldsymbol{z}_4, \boldsymbol{z})$ *(right).*

[5] C. Bardos, J. Garnier, and G. Papanicolaou, Identification of Green's functions singularities by cross correlation of noisy signals, Inverse Problems, 24 (2008), 015011.

[6] L. Borcea, G. Papanicolaou, C. Tsogka, and J. G. Berrymann, Imaging and time reversal in random media, Inverse Problems, 18 (2002), 1247–1279.

[7] Y. Colin de Verdière, Semiclassical analysis and passive imaging, Nonlinearity, 22 (2009), R45–75.

[8] J.-P. Fouque, J. Garnier, G. Papanicolaou, and K. Sølna, *Wave Propagation and Time Reversal in Randomly Layered Media*, Springer, New York, 2007.

[9] J. Garnier and G. Papanicolaou, Passive sensor imaging using cross correlations of noisy signals in a scattering medium, SIAM J. Imaging Sciences, 2 (2009), 396–437.

[10] J. Garnier and G. Papanicolaou, Resolution analysis for imaging with noise, Inverse Problems, 26 (2010), 074001.

[11] J. Garnier and K. Sølna, Filtered Kirchhoff migration of cross correlations of ambient noise signals, to appear in Inverse Problems and Imaging.

[12] J. Huang, N. Ohnishi, and N. Sugie, Building ears for robots: sound localization and separation, Artificial Life and Robotics, 1 (2007), 157–163.

[13] E. Martinson, Hiding the acoustic signature of a mobile robot, Intelligent Robots and Systems, IEEE/RSJ International Conference, San Diego 2007, 985–990.

[14] E. Martinson and A. Schultz, Discovery of sound sources by an autonomous mobile robot, J. Autonomous Robots, 27 (2009), 221–237.

[15] K. Nakadai, D. Matsuura, H. G. Okuno, and H. Kitano, Applying scattering theory to robot audition system: robust sound source localization and extraction, Proceedings of the 2003 IEEE/RSJ Intl. Conference on Intelligent Robots and Systems, Las Vegas 2003, 1147–1152.

[16] A. F. Nikiforov and V. B. Uvarov, *Special Functions of Mathematical Physics. A Unified Introduction with Applications*, Birkhäuser, Basel, 1988.

[17] N.M. Shapiro, M. Campillo, L. Stehly, and M. H. Ritzwoller, High-resolution surface wave tomography from ambient noise, Science, 307 (2005), 1615–1618.

[18] L. Stehly, M. Campillo, and N. M. Shapiro, A study of the seismic noise from its long-range correlation

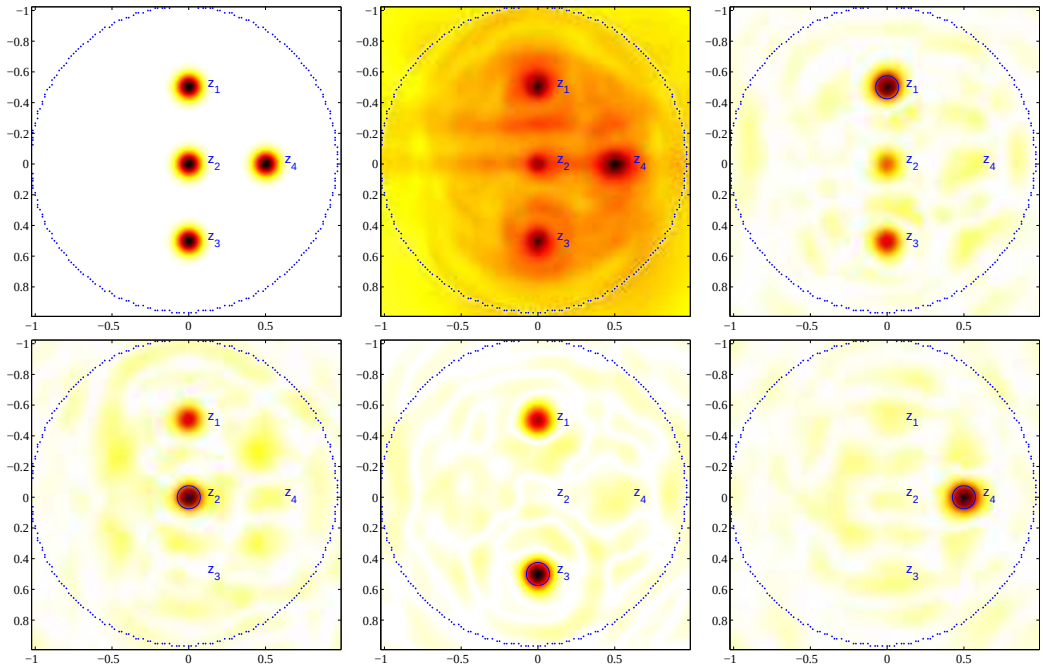

FIG. 5.2. *Test 4: four correlated extended sources centered at* $(\boldsymbol{z}_j)_{j=1,\dots,4}$ *with* $T = 8$, $\omega_{\max} = 1000$, $N_x = 2^8$, *and* $N_t = 2^{11}$. *Top line:* $K(\boldsymbol{z})$ *(left),* $\mathcal{I}_W$ *with* $W(\omega) = |\omega|^3 \mathbf{1}_{|\omega|<\omega_{\max}}$ *(middle),* $\boldsymbol{z} \to \mathcal{J}_W(\boldsymbol{z}_1, \boldsymbol{z})$ *(right). Bottom line:* $\boldsymbol{z} \to \mathcal{J}_W(\boldsymbol{z}_2, \boldsymbol{z})$ *(left),* $\boldsymbol{z} \to \mathcal{J}_W(\boldsymbol{z}_3, \boldsymbol{z})$ *(middle),* $\boldsymbol{z} \to \mathcal{J}_W(\boldsymbol{z}_4, \boldsymbol{z})$ *(right).*

properties, J. Geophys. Res., 111 (2006), B10306.

[19] R. Snieder, Extracting the Green's function from the correlation of coda waves: A derivation based on stationary phase, Phys. Rev. E, 69 (2004), 046610.

[20] R. Snieder, Extracting the Green's function of attenuating heterogeneous acoustic media from uncorrelated waves, J. Acoust. Soc. Am., 121 (2007), 2637–2643.

[21] J.M. Valin, F. Michaud, J. Rouat, and D. Létourneau, Robust sound source localization using a microphone array on a mobile robot, Intelligent Robots and Systems, IEEE/RSJ International Conference, 1228–1233, 2003.